BEILSTEIN JOURNAL OF ORGANIC CHEMISTRY

Ionic multiresonant thermally activated delayed fluorescence emitters for light emitting electrochemical cells

Merve Karaman[1,2], Abhishek Kumar Gupta[2,3], Subeesh Madayanad Suresh[2], Tomas Matulaitis[2], Lorenzo Mardegan[4], Daniel Tordera[*4], Henk J. Bolink[4], Sen Wu[2], Stuart Warriner[5], Ifor D. Samuel[3] and Eli Zysman-Colman[*2]

Full Research Paper

Open Access

Address:
[1]Department of Material Science and Engineering, Faculty of Engineering and Architecture, Izmir Katip, Celebi University, Cigli, 35620-Izmir, Turkey, [2]Organic Semiconductor Centre, EaStCHEM School of Chemistry, University of St Andrews, St Andrews, UK, KY16 9ST, [3]Organic Semiconductor Centre, SUPA School of Physics and Astronomy, University of St Andrews, St Andrews KY16 9SS, UK, [4]Instituto de Ciencia Molecular (ICMol), Universidad de Valencia, C/Catedrático J. Beltrán 2, 46980 Paterna (Valencia), Spain and [5]School of Chemistry, University of Leeds, Woodhouse Lane, Leeds, UK

Email:
Daniel Tordera[*] - daniel.tordera@uv.es; Eli Zysman-Colman[*] - eli.zysman-colman@st-andrews.ac.uk

* Corresponding author

Keywords:
electroluminescence; light-emitting electrochemical cells; multiresonance; purely organic emitters; thermally activated delayed fluorescence

Beilstein J. Org. Chem. **2022,** *18,* 1311–1321.
https://doi.org/10.3762/bjoc.18.136

Received: 24 June 2022
Accepted: 08 September 2022
Published: 22 September 2022

This article is part of the thematic issue "Organic TADF materials design".

Associate Editor: P. J. Skabara

Abstract

We designed and synthesized two new ionic thermally activated delayed fluorescent (TADF) emitters that are charged analogues of a known multiresonant TADF (MR-TADF) compound, **DiKTa**. The emission of the charged derivatives is red-shifted compared to the parent compound. For instance, **DiKTa-OBuIm** emits in the green (λ_{PL} = 499 nm, 1 wt % in mCP) while **DiKTa-DPA-OBuIm** emits in the red (λ_{PL} = 577 nm, 1 wt % in mCP). In 1 wt % mCP films, both emitters showed good photoluminescence quantum yields of 71% and 61%, and delayed lifetimes of 316.6 µs and 241.7 µs, respectively, for **DiKTa-OBuIm** and **DiKTa-DPA-OBuIm**, leading to reverse intersystem crossing rates of 2.85×10^3 s^{-1} and 3.04×10^3 s^{-1}. Light-emitting electrochemical cells were prepared using both **DiKTa-OBuIm** and **DiKTa-DPA-OBuIm** as active emitters showing green (λ_{max} = 534 nm) and red (λ_{max} = 656 nm) emission, respectively.

Introduction

Light-emitting electrochemical cells (LEECs) are thin film light-emitting devices typically consisting of an emissive layer containing ionic species that facilitate charge transport and an emissive semiconductor material. The emissive layer is sandwiched between two air-stable electrodes [1]. Upon application of an external bias the ions in the active layer migrate to the corresponding electrodes, resulting in the formation of electrical double layers (EDLs) at the interface of the electrodes. The EDLs facilitate charge injection into the emissive layer regardless of the energy levels of the electroactive species and work function of the electrodes. Injection of electrons and holes creates oxidized and reduced species near the anode and cathode, respectively. These oxidized and reduced species are stabilized by the ions to form a p-i-n junction in the bulk of the emissive layer and emission takes place within the intrinsic region [2-6].

Two families of widely investigated emitters for LEECs are ionic transition metal complexes (iTMCs) [7-10] and conjugated polymers (CPs) [4]. From the early use of ruthenium(II) complexes, a significant amount of research has focussed on developing high-performance iTMC-based LEECs [11,12], with iridium(III) complexes typically showing the greatest potential. A detracting feature of many iTMC LEECs is the use of scarce noble metal complexes. Despite the enormous number of low molecular weight organic emitters designed for use in organic light-emitting diodes (OLEDs), relatively little attention has been devoted to the design of ionic small molecule (SM) [13] organic emitters for LEECs. The majority of the reported SM emitters for LEECs are fluorescent in nature and so the internal quantum efficiency (IQE) of the device is limited to 25% [13]. Thermally activated delayed fluorescent (TADF) emitters are one class of purely organic materials that can harvest triplet excitons in electroluminescent (EL) devices through a triplet to singlet reverse intersystem crossing (RISC) upconversion process [14]. Indeed, OLEDs using TADF emitters can achieve up to 100% IQE, comparable to devices using phosphorescent emitters [15].

Purely organic TADF emitters have not been widely investigated for use in LEECs. We reported the first organic TADF LEEC, **I** (Figure 1a, original compound **2** in [16]), in 2015 by adapting the structure of the known TADF emitter 2CzPN with imidazolium groups [16,17] (Figure 1a). The LEEC devices showed a maximum external quantum efficiency (EQE_{max}) of 0.39%, a maximum brightness (B_{max}) of 13 cd m^{-2}, and a peak electroluminescence (λ_{EL}) at 538 nm. The device performance suffered when the emissive layer was doped with an ionic liquid (EQE_{max} = 0.12%, B_{max} = 10 cd m^{-2}), which was incorporated to increase charge mobility within the emissive layer. We later showed that this emitter could act as host material in combination with a cyanine dye emitter [18]. The EQE_{max} for this host–guest device was higher than for the non-doped device, at 2.0% demonstrated 100% exciton utilization efficiency in the device and efficient energy transfer from the host to the guest cyanine emitter. Deep blue emission in LEECs is challenging. We also reported a blue-emitting LEEC employing a cationic sulfone-based donor–acceptor TADF emitter, **imCzDPS** (λ_{PL} = 440 nm, Φ_{PL} = 44%, neat film) [19]. The EL of the LEEC was red-shifted at λ_{EL} of 470 nm compared to the PL. Following these initial reports Edman and co-workers demonstrated how neutral TADF small molecules [20], polymers [21], and dendrimers [22] could be employed in LEECs where the emissive layer also contained an inorganic salt and a conducting polymer. Recently, a step-change in device performance were achieved by He et al. who employed a cationic TADF compound that possesses low-lying through-space and through-bond charge transfer excited states [23]. The LEEC showed a green EL with a peak brightness of 572 cd m^{-2} and an EQE_{max} of 6.8% at 4.0 V. The half-life of their device reached 218 h at a brightness of 162 cd m^{-2}. Recently, Su et al. reported two ionic TADF emitters incorporating a pyridinium moiety, **Pym-CZ** and **Pym-tBuCZ** as the acceptor and carbazole or *tert*-butylcarbazole as donor groups [24]. **Pym-CZ** showed red emission in dichloromethane (λ_{PL} = 691 nm, Φ_{PL} = 43%) and in the neat film (λ_{PL} = 583 nm, Φ_{PL} = 15%). The emission is further red-shifted and attenuated in **Pym-tBuCZ** in dichloromethane (λ_{PL} = 740 nm, Φ_{PL} = 8%) and in the neat film (λ_{PL} = 593 nm, Φ_{PL} = 6%). The LEECs with **Pym-CZ** (λ_{EL} = 599 nm, B_{max} = 8.69 cd m^{-2}, EQE_{max} = 0.91%) and **Pym-tBuCZ** (λ_{EL} = 618 nm, B_{max} = 1.96 cd m^{-2}, EQE_{max} = 0.05%) are the first examples of orange-red devices employing purely organic intrinsically ionic TADF emitters. Though these reports hint at the potential of TADF emitters in LEECs, the emission in these devices is typically broad, reflective of the charge transfer (CT) character of the emission, and so colour purity suffers.

Narrowband emission has, however, been demonstrated in multiresonant TADF (MR-TADF) materials. MR-TADF compounds, first introduced by Hatakeyama and co-workers, are typically p- and n-doped nanographenes [25,26]. OLEDs using MR-TADF emitters can simultaneously achieve narrowband emission and very high EQE_{max}. Inspired by our recent work on neutral MR-TADF emitters for OLEDs [27,28], we designed two charged analogues of **DiKTa** [29] (Figure 1b), to make them amenable for use as emitters in LEECs, **DiKTa-OBuIm** and **DiKTa-DPA-OBuIm** (Figure 1c). In 1 wt % doped mCP films, **DiKTa-OBuIm** emits in the green region (λ_{PL} = 499 nm, Φ_{PL} = 71%, 1 wt % in mCP) and **DiKTa-DPA-OBuIm** is a red emitter (λ_{PL} = 577 nm, Φ_{PL} = 61%, 1 wt % in mCP). The pres-

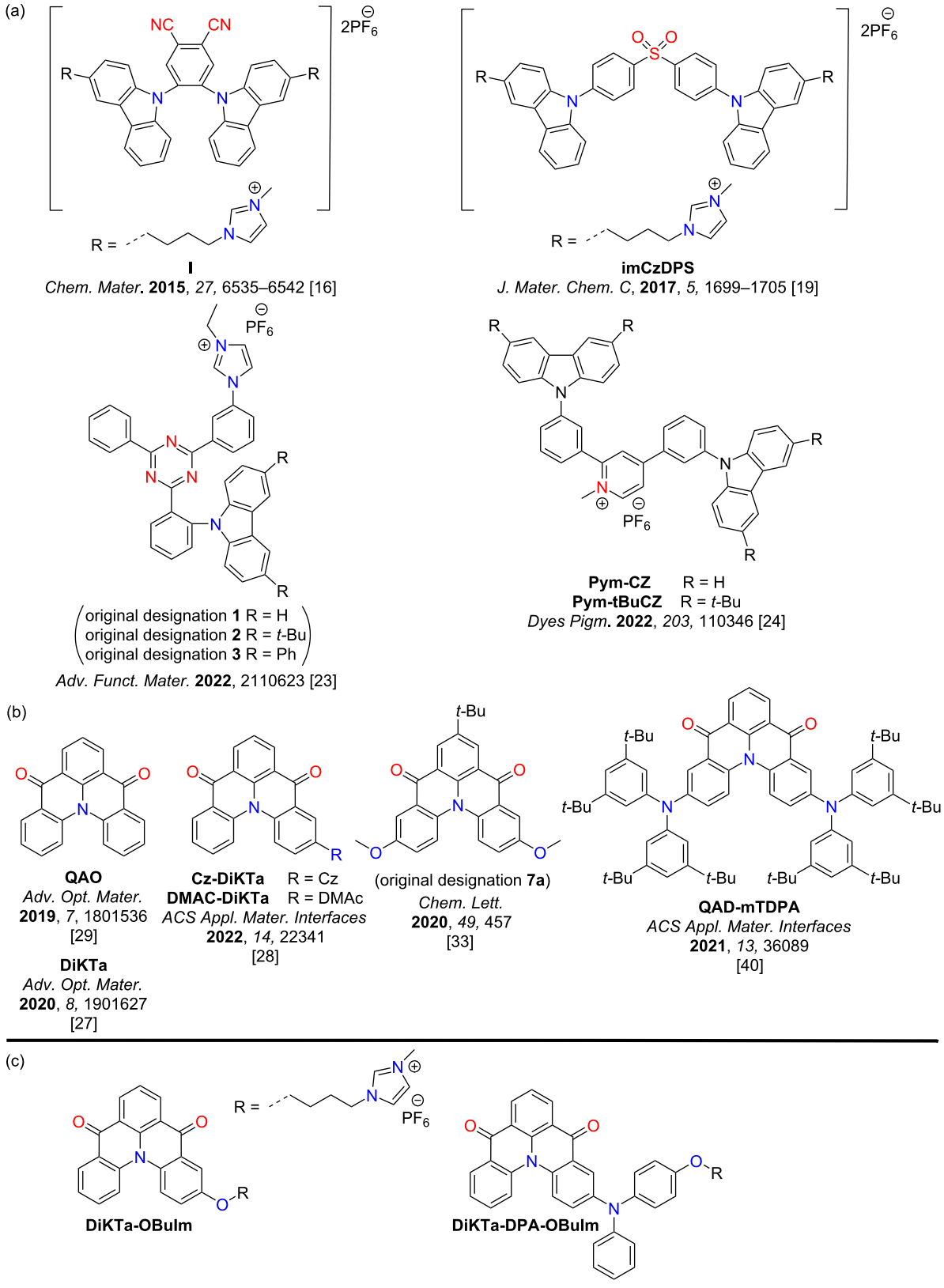

Figure 1: Chemical structures of (a) reported ionic TADF emitters for LEECs, (b) the MR-TADF emitter **DiKTa** and selected derivatives, and (c) the ionic emitters in this work.

ence of the DPA group in **DiKTa-DPA-OBuIm** transforms this compound from one that is MR-TADF to one that is better described as a donor–acceptor TADF, which is reflected in the red-shifted and broadened emission [28].

Results and Discussion

DiKTa-OBuIm was obtained in three steps (Scheme 1) in 23% overall yield. First, hydrolysis of **1**, in situ conversion to the acyl chloride and subsequent Lewis acid-promoted Friedel–Crafts acylation reaction produced compound **2** (Scheme 1), where the $AlCl_3$ was also responsible for the demethylation. Compound **2** was then subjected to monoalkylation with 1,4-dibromobutane in moderate yield, followed by a second alkylation step with 1-methylimidazole in very good yield. **DiKTa-OBuIm** was isolated as its hexafluorophosphate salt following anion metathesis with NH_4PF_6. **DiKTa-DPA-OBuIm** was obtained also in three steps at 35% overall yield from compound **4** using a similar synthetic strategy, which itself was synthesized from **Br-DiKTa** [28] following a Buchwald–Hartwig coupling. Details of the synthesis are found in Supporting Information File 1. The identity and purity of the molecules were verified using a combination of ^1H and

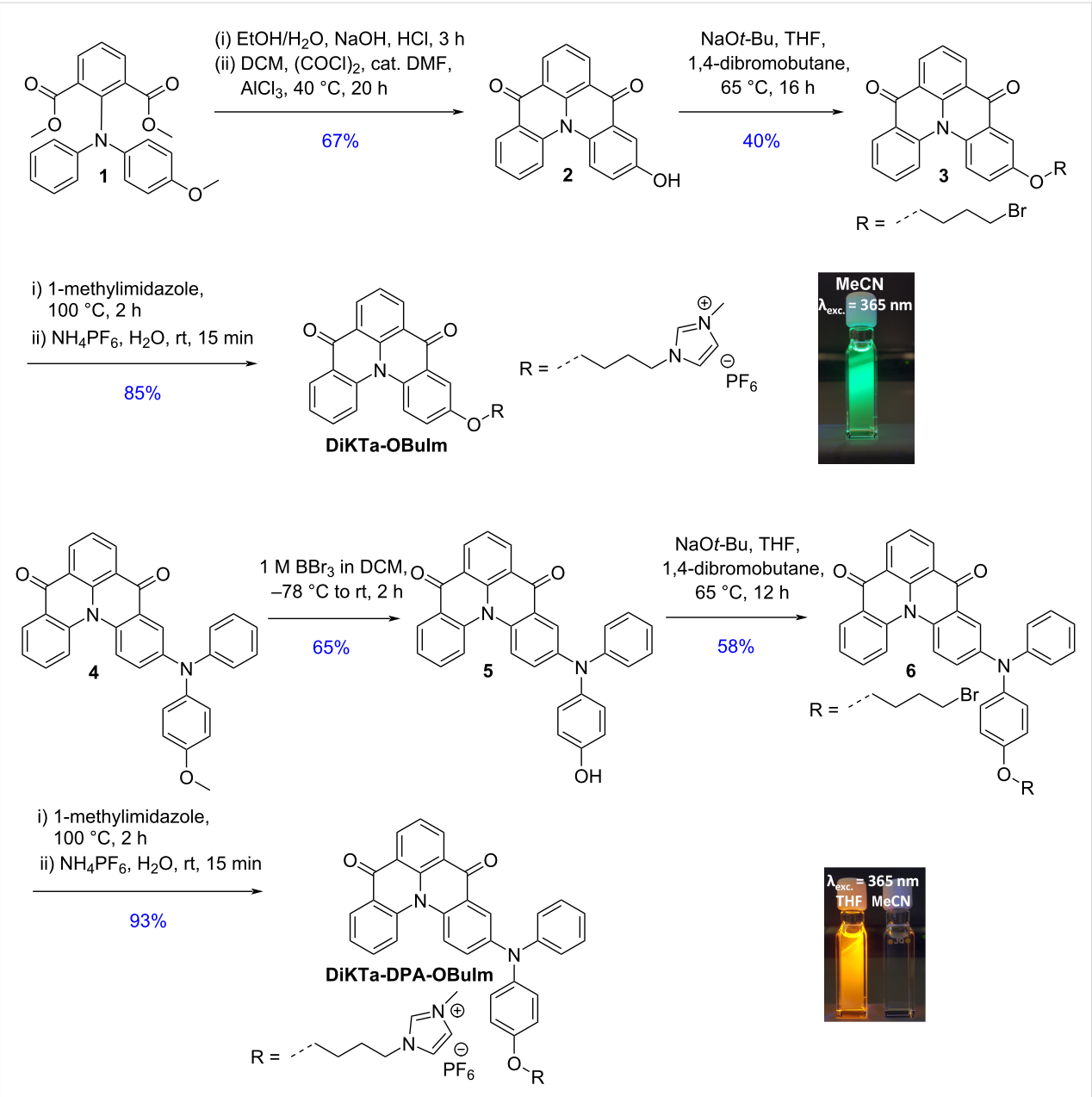

Scheme 1: Synthesis of **DiKTa-OBuIm** and **DiKTa-DPA-OBuIm**.

^{13}C NMR spectroscopy, high resolution mass spectrometry (HRMS) (Figures **S1–S24** in Supporting Information File 1), and melting point analysis.

We modelled the electron density distribution in **DiKTa-OBuIm** and **DiKTa-DPA-OBuIm** using density functional theory (DFT) calculations in the ground state, at the PBE0/6-31G(d,p) level of theory in the gas phase (Figure 2a). The calculations were based on model systems, **DiKTa-OMe** and **DiKTa-DPA-OMe**, respectively, wherein we replaced the imidazolium side chain of **DiKTa-OBuIm** and **DiKTa-DPA-OBuIm**, respectively, with a methyl group [30]. Compared to **DiKTa** (HOMO = −6.20 eV, LUMO = −2.23 eV, ΔE_g = 3.97 eV), both emitters possess a smaller HOMO–LUMO gap. The HOMO is more strongly affected by the incorporation of donor units [28]. For instance, in the case of **Cz-DiKTa** and **DMAC-DiKTa** the HOMO is destabilized by 0.47 eV and 0.94 eV, respectively, compared to **DiKTa** [28]. The lowest unoccupied molecular orbital (LUMO) for both compounds is localized on the **DiKTa** core (Figure S25 in Supporting Information File 1). This orbital is only slightly stabilized in **DiKTa-DPA-OMe** due to the presence of the more strongly electron-donating DPA group. The highest occupied molecular orbital (HOMO) in **DiKTa-OMe** is also localized on the **DiKTa** core and the electron density distribution of this molecule is reminiscent of that of a MR-TADF compound and is nearly identical to that of the parent emitter, **DiKTa** [27] (Figure S25 in Supporting Information File 1). There is a very large change in both the electron density distribution and the HOMO energy between the two emitters. For **DiKTa-DPA-OMe**, the HOMO is mainly localized on the DPA unit but with some delocalization onto the **DiKTa** core, resulting in a destabilization of this orbital from −5.91 eV in **DiKTa-OMe** to −5.19 eV in **DiKTa-DPA-OMe**. The HOMO–LUMO gap, ΔE_g, thus decreases to 3.08 eV compared to that of **DiKTa-OMe** (3.74 eV). The excited states were modelled using spin-component scaling second-order approximate coupled-cluster (SCS-CC2) in tandem with the cc-pVDZ basis set (Table S1 in Supporting Information File 1). Figure 2b shows the difference density plots for singlet (S) and triplet (T) excited states for **DiKTa-OMe** and **DiKTa-DPA-OMe**. Compared to **DiKTa** (S_1 = 3.45 eV, T_1 = 3.18 eV, f = 0.20, ΔE_{ST} = 0.27 eV) [28], the lowest-lying singlet (S_1) and triplet (T_1) states are stabilized in the case of **DiKTa-OMe**, while the singlet–triplet energy gap, ΔE_{ST}, remained the same at 0.27 eV. The nature of S_1 and T_1 resemble to those of its parent **DiKTa** and so this compound is

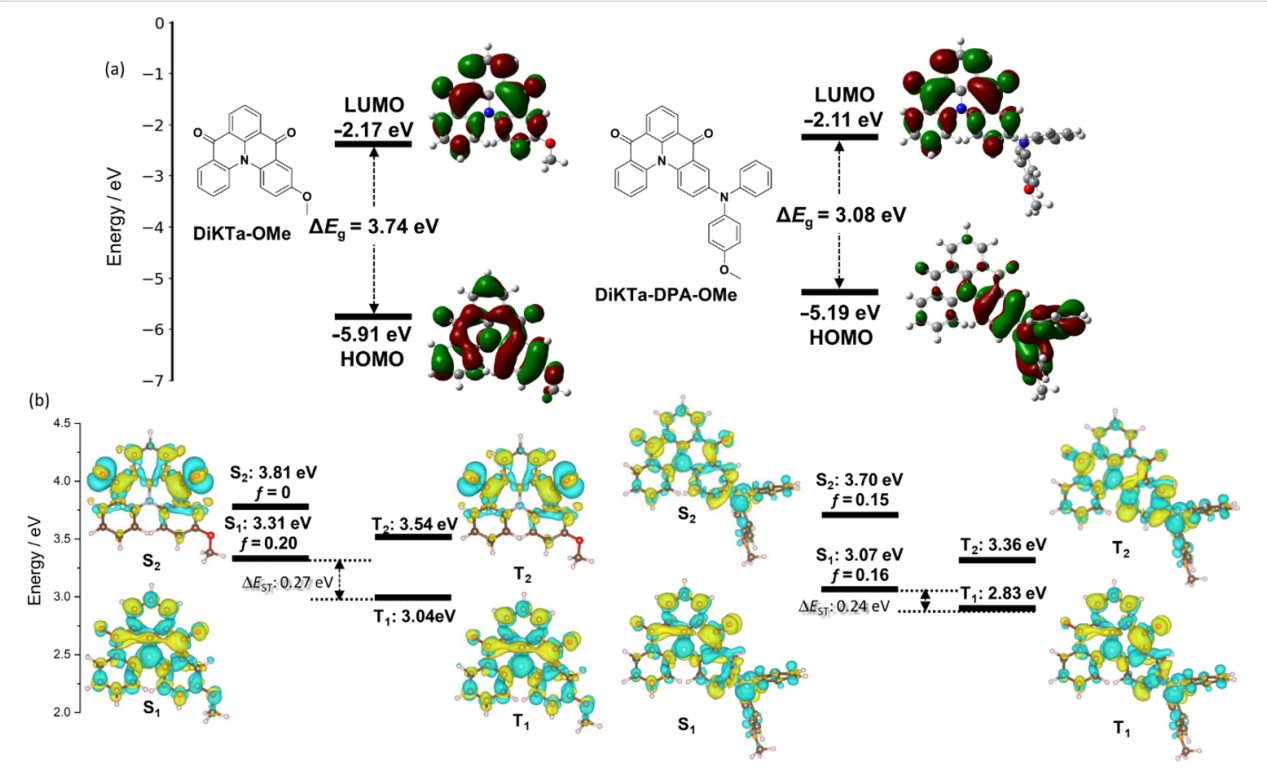

Figure 2: (a) HOMO and LUMO electron density distribution and orbital energies of **DiKTa-OMe** and **DiKTa-DPA-OMe** calculated at the PBE0/6-31G(d,p) level of theory in the gas phase, isovalue = 0.02; (b) difference density plots and energies for the two lowest-lying singlet and triplet excited states for **DiKTa-OMe** and **DiKTa-DPA-OMe** calculated at SCS-CC2/cc-pVDZ in the gas phase (isovalue = 0.001). The blue color represents an area of decreased electron density, and yellow represents an increased electron density between the ground and excited states; *f* denotes the oscillator strength for the transition to the excited singlet state.

likely to behave as a MR-TADF emitter. The nature of the S_2 state is n–π* in **DiKTa-OMe**. The excited state picture of **DiKTa-DPA-OMe** is different to that of other reported D–A-type systems containing **DiKTa** as the acceptor [28]. Long range charge transfer is not apparent here and instead the coupled cluster calculations predict a compound that is MR-TADF but where the electron density distribution is delocalized over the entire molecule. Compared to **DiKTa-OMe**, both S_1 and T_1 of **DiKTa-DPA-OMe** are stabilized to 3.07 eV and 2.83 eV, respectively. The ΔE_{ST} decreases to 0.24 eV and there is no intermediate triplet state. The trend of stabilized S_1 and T_1 states when a donor group decorates the **DiKTa** core (S_1 = 3.45 eV, T_1 = 3.18 eV) has been previously observed in reported emitters such as **Cz-DiKTa** (S_1 = 3.35 eV, T_1 = 3.09 eV) and **DMAC-DiKTa** (S_1 = 3.43 eV, T_1 = 3.17 eV) [28]. We also calculated the charge transfer character of each excited state, focussing on the distance of charge transfer (D_{CT}). When considering the S_1 excited state, there is an increase in CT character moving from **DiKTa**, **DiKTa-OMe**, and **DiKTa-DPA-OMe** (D_{CT} = 1.45 Å, 1.81 Å, and 3.34 Å, respectively) reflected in the increased donor strength.

The electrochemical properties of **DiKTa-OBuIm** and **DiKTa-DPA-OBuIm** were investigated by cyclic voltammetry (CV) and differential pulse voltammetry (DPV) in acetonitrile with 0.1 M tetra-*n*-butylammonium hexafluorophosphate as the supporting electrolyte (Figure 3a and Table S2 in Supporting Information File 1). The oxidation and reduction of both emitters showed good reversibility, which is beneficial for better performance in LEEC devices [31]. The oxidation potentials, E_{ox}, determined from the peak value of the first DPV curve are 1.05 V and 0.44 V for **DiKTa-OBuIm** and **DiKTa-DPA-OBuIm**, respectively, which correspond to HOMO energy levels of −5.85 eV and −5.24 eV, respectively. The trend of a destabilized HOMO energy level from **DiKTa-OBuIm** to **DiKTa-DPA-OBuIm** is predicted by DFT calculations. **DiKTa** possesses an oxidation potential of 1.66 V and an associated HOMO energy level of −5.93 eV. The reduction potentials, E_{red}, are −1.67 V and −1.61 V, respectively, for **DiKTa-OBuIm** and **DiKTa-DPA-OBuIm**. The corresponding LUMO levels are −3.13 eV and −3.18 eV for **DiKTa-OBuIm** and **DiKTa-DPA-OBuIm**, respectively. The LUMO values of both emitters match that of **DiKTa** (−3.11 eV), which suggests that reduction occurs on the **DiKTa** core in both compounds, a contention corroborated by the DFT calculations. The electrochemical gap reduced from 2.72 V in **DiKTa-OBuIm** to 2.06 V in **DiKTa-DPA-OBuIm**, a trend that is in line with the DFT calculations.

Figure 3b shows the solution-state photophysical properties of **DiKTa-OBuIm** and **DiKTa-DPA-OBuIm** in acetonitrile and the data are compiled in Table 1. The lowest energy absorption band for **DiKTa-OBuIm** at 453 nm ($\varepsilon = 17 \times 10^3$ M^{-1} cm^{-1}) is red-shifted and slightly more intense than that of the parent **DiKTa** at 436 nm, ($\varepsilon = 14 \times 10^3$ M^{-1} cm^{-1}) [27] owing to the increased conjugation in **DiKTa-OBuIm**. For the emitter **7a** (Figure 1b) [33] reported by Yan et al. the red-shift of the lowest energy absorption band was more pronounced than that in **DiKTa-OBuIm**. This band is assigned to a short-range charge transfer transition (SRCT) that is a hallmark characteristic in MR-TADF compounds [28]. The Stokes shift is 54 nm (2361 cm^{-1}) for **DiKTa-OBuIm**. The lowest energy absorption band in **DiKTa-DPA-OBuIm** is red-shifted and less intense ($\varepsilon = 6 \times 10^3$ M^{-1} cm^{-1}) compared to **DiKTa-OBuIm**, in line

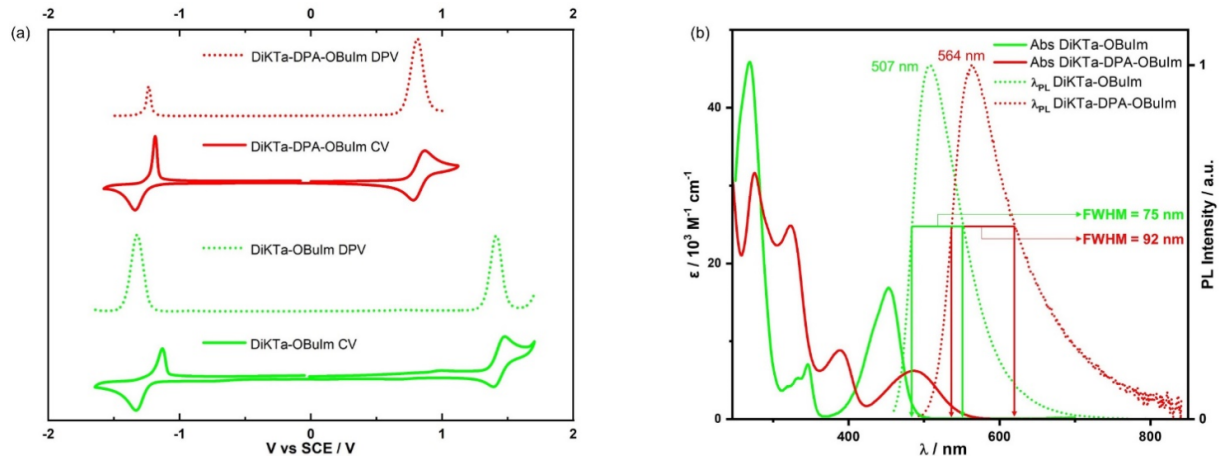

Figure 3: (a) Cyclic and differential pulse voltammograms measured in degassed MeCN with 0.1 M [*n*-Bu_4N]PF_6 as the supporting electrolyte and Fc^+/Fc as the internal reference (0.38 V vs SCE) [32]. Scan rate = 100 mV s^{-1}; (b) solution-state photophysical measurements: absorption and steady-state emission spectra at 300 K measured in MeCN. λ_{exc} = 453 nm for **DiKTa-OBuIm** and λ_{exc} = 488 nm for **DiKTa-DPA-OBuIm**.

Table 1: Photophysical properties of **DiKTa-OBuIm** and **DiKTa-DPA-OBuIm**.

Compound	Medium	λ_{Abs}[a] [nm]	λ_{PL}[b] [nm]	FWHM[c] [nm]	E_{S1}[d] [eV]	E_{T1}[d] [eV]	ΔE_{ST}[e] [eV]
DiKTa-OBuIm	sol.[f]	453 (17)	507	75	2.66	2.41	0.25
	film[g]	–	500	66	2.65	2.45	0.20
DiKTa-DPA-OBuIm	sol.[f]	488 (6)	563	92	–	–	–
	film[g]	–	578	95	2.40	2.21	0.19
	Φ_{PL}[h] [%]	τ_p[i] [ns]	τ_d[i] [µs]	k_{ISC}[j] [s^{-1}] ($\times 10^7$)	k_{RISC}[j] [s^{-1}] ($\times 10^3$)	k_{s_r}[j] [s^{-1}] ($\times 10^7$)	k_{s_nr}[j] [s^{-1}] ($\times 10^7$)
DiKTa-OBuIm	48[a]	14.3[a]	–	–	–	–	–
	71 (57)[b]	8.7[b]	316.6[b]	3.59 ± 1.3	2.85 ± 1.1	6.60	2.69
DiKTa-DPA-OBuIm	11[a]	12.7[a]	–	–	–	–	–
	61 (53)[b]	14.1[b]	241.7[b]	2.21 ± 1.2	3.04 ± 1.7	3.78	2.38

[a]Lowest energy absorbance band, absorptivity (ε) in parentheses (/ × 10^3 M^{-1} s^{-1}). [b]Steady-state emission maximum at 300 K; λ_{exc} = 340 nm. [c]Full width at half maximum of the emission peak. [d]S_1 and T_1 energies were obtained from the onsets of the respective prompt fluorescence (delay: 1 ns; gate time: 100 ns) and phosphorescence spectra (delay: 1 ms; gate time: 9 ms) at 77 K; λ_{exc} = 343 nm. [e]$\Delta E_{ST} = E(S_1) - E(T_1)$. [f]In MeCN solutions ($10^{-6}$ M). [g]Measured in spin-coated thin films consisting of 1.0 wt % emitter in mCP; λ_{exc} = 340 nm. [h]Φ_{PL} in solutions were measured by the relative method using quinine sulfate as a standard (Φ_r = 54.6% in 1 N H_2SO_4) [38], while absolute Φ_{PL} of thin films were measured using an integrating sphere; λ_{exc} = 340 nm under nitrogen and the values in parentheses are in the presence of O_2. [i]Prompt and delayed lifetimes in solutions and thin films obtained by TCSPC and MCS, λ_{exc} = 379 nm. [j]Intersystem and reverse intersystem crossing rates were calculated using the steady-state approximation method as described in literature [39].

with its decreased oscillator strength (vide supra). According to the calculations (vide supra), the S_1 excited state is also SRCT, but with larger long-range charge transfer (LRCT) content. Owing to the relative flexibility around the DPA donor unit, the Stokes shift is larger at 75 nm (2761 cm^{-1}). **DiKTa-OBuIm** and **DiKTa-DPA-OBuIm** exhibited broad green (λ_{PL} = 507 nm, FWHM = 75 nm) and red (λ_{PL} = 563 nm, FWHM = 92 nm) emissions in MeCN, respectively, which is larger than **DiKTa** (46 nm in MeCN) [27] in line with the greater LRCT character for these emitters; this observation has been noted for other donor decorated MR-TADF emitters [34-36]. The photoluminescence quantum yield, Φ_{PL}, in MeCN for **DiKTa-OBuIm** is 48% which decreases in air to 34%. The emission is much weaker in **DiKTa-DPA-OBuIm**, reflecting both the smaller oscillator strength of the transition to S_1 and the greater non-radiative decay due to the energy gap law (Φ_{PL} = 11% and 7% under vacuum and in air, respectively) in MeCN [37]. The S_1 and T_1 levels were measured from the onsets of fluorescence (2.66 eV) and phosphorescence spectra (2.41 eV) in 2-MeTHF glass at 77 K (Figure S26, Supporting Information File 1). **DiKTa-OBuIm** possesses a ΔE_{ST} of 0.25 eV. Unfortunately, **DiKTa-DPA-OBuIm** was insoluble in 2-MeTHF and so the measurement could not be made. No delayed component was observed in MeCN solution under vacuum for either of the compounds (Figure S27 in Supporting Information File 1).

The thin film PL behavior of both emitters was then assessed in 1 wt % doped film in 1,3-di-9-carbazolylbenzene (mCP) (Figure 4). At this doping concentration, the photophysical

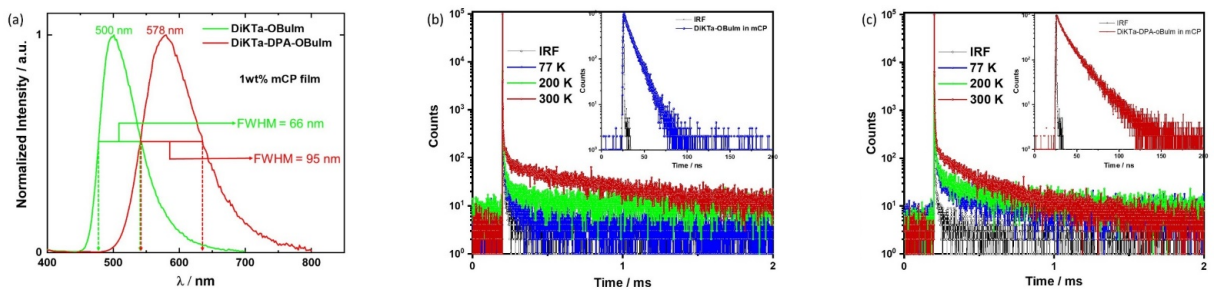

Figure 4: (a) Steady-state emission spectra of **DiKTa-OBuIm** and **DiKTa-DPA-OBuIm** in 1 wt % doped mCP films, $\lambda_{exc.}$ = 340 nm; (b) temperature-dependent time resolved PL decays of **DiKTa-OBuIm** in 1 wt % doped mCP films. Inset: prompt PL decay of **DiKTa-OBuIm;** (c) temperature-dependent time resolved PL decays of **DiKTa-DPA-OBuIm** in 1 wt % doped mCP films. Inset: prompt PL decay of **DiKTa-DPA-OBuIm**, $\lambda_{exc.}$ = 379 nm.

properties should reflect monomolecular entities. Emission was observed at 500 nm (FWHM = 66 nm) and 578 nm (FWHM = 95 nm) for **DiKTa-OBuIm** and **DiKTa-DPA-OBuIm**, respectively. The emission spectrum of **DiKTa-OBuIm** is slightly blue-shifted and narrower than that in MeCN, which is expected due to the higher polarity of the solvent than mCP. Surprisingly, for **DiKTa-DPA-OBuIm** the emission is red-shifted by 14 nm, and with negligible change in the FWHM. This suggests that the conformation of the emitter in the solid state is slightly more conjugated than that in solution or that there are specific host–guest interactions with the DPA unit that perturbs the energy of the excited state. The emission is broader than that of a structurally similar emitter, **QAD-mTDPA**, a derivative of **DiKTa** containing two DPA substituents, reported by Zhang et al. [40] The structure of **QAD-mTDPA** (λ_{PL} = 587 nm, FWHM = 62 nm, Φ_{PL} = 97%, ΔE_{ST} = 0.33 eV, τ_D = 269 μs, 1.5 wt % CBP) is shown in Figure 1b. Both emitters showed red-shifted and broadened emission compared to that of **DiKTa** (λ_{PL} = 466 nm, FWHM = 40 nm, Φ_{PL} = 70%, ΔE_{ST} = 0.20 eV, τ_D = 168 μs, 2 wt % mCP) in the same host [28]. Both emitters exhibited high Φ_{PL} values in the mCP film at 71% and 61% under nitrogen, and these reduced to 57% and 53% in air for **DiKTa-OBuIm** and **DiKTa-DPA-OBuIm**, respectively. As neat thin films, the emission for both compounds are red-shifted and significantly quenched (Figure S28 in Supporting Information File 1); indeed, the Φ_{PL} for the neat film of **DiKTa-OBuIm** is only 9% while we could not ascertain a reliable value for **DiKTa-DPA-OBuIm**. Severe aggregation-caused quenching of the emission in the neat film was also observed for **DiKTa** (Φ_{PL} = 11%, under N_2) [27]. The S_1 and T_1 levels were measured from the onsets of fluorescence and phosphorescence spectra in the 1 wt % doped mCP film at 77 K (Figure S29 in Supporting Information File 1). The corresponding ΔE_{ST} values are 0.20 eV and 0.19 eV, respectively, for **DiKTa-OBuIm** and **DiKTa-DPA-OBuIm**, which are nearly same to that reported for **DiKTa** (ΔE_{ST} = 0.20 eV) [28]. Experimental ΔE_{ST} values are smaller than those computationally predicted (0.27 eV and 0.24 eV, respectively for **DiKTa-OBuIm** and **DiKTa-DPA-OBuIm**). However, the trend of decreasing ΔE_{ST} is in line to the findings from DFT. The temperature dependent time-resolved PL decays in the 1 wt % doped mCP films are presented in Figure 4b and c. Both emitters show prompt and delayed emission components with an enhancement of the delayed emission with increasing temperature, a feature of TADF. Unlike the delayed emission lifetime of **DiKTa** (15 μs in 3.5 wt % mCP, 23 μs in PhMe) [27], and its derivatives such as **Cz-DiKTa** (τ_D = 196 μs, 2 wt % mCP), **DMAC-DiKTa** (τ_D = 6.6 μs, 2 wt % mCP), and **QAD-mTDPA** (τ_D = 168 μs, in 2 wt % mCP) in Figure 1b [28,40], the delayed lifetimes from **DiKTa-OBuIm** and **DiKTa-DPA-OBuIm** are long at 317 μs and 242 μs, respectively. RISC rate constants, k_{RISC}, were calculated for both emitters, which are 2.85×10^3 s^{-1} and 3.04×10^3 s^{-1}, respectively for **DiKTa-OBuIm** and **DiKTa-DPA-OBuIm**, compared to that of **DiKTa** (4.6×10^4 s^{-1}) in toluene [27,39].

Light-emitting electrochemical cells

LEECs were fabricated using **DiKTa-OBuIm** and **DiKTa-DPA-OBuIm** as emitters. The device stack was the following: ITO/PEDOT:PSS/emitter/Al (where ITO is indium tin oxide; PEDOT:PSS is poly(3,4-ethylenedioxythiophene):poly(styrenesulfonate)). The PEDOT:PSS and the emitter layers were prepared from solution and the device was finished with an evaporated Al top contact. Details of the LEEC fabrication can be found in the General Methods section of Supporting Information File 1. Driven by their promising Φ_{PL} LEEC devices using **DiKTa-OBuIm** and **DiKTa-DPA-OBuIm** as 1 wt % doped films in mCP as the emitter layer were prepared. The devices showed no turn-on, both in lifetime measurements and in current density and luminance versus voltage sweeps (*JVL*) up to 8 V. Most likely the low content of ionic species in the neutral matrix hindered the required ionic transport for LEEC operation. To solve this, we fabricated devices adding an ionic liquid (lithium hexafluorophosphate ($LiPF_6$) or 1-butyl-3-methylimidazolium hexafluorophosphate ($BMIM:PF_6$) in a 4 to 1 molar ratio) and, in some cases, an electrolyte matrix (PEO (polyethylene oxide)), to improve the ionic mobility on the active film [5,41]. However, despite these efforts, still no emission was observed when the devices were biased. Next, neat films of **DiKTa-OBuIm** and **DiKTa-DPA-OBuIm** were directly used as active layers. Non-doped small molecule films have shown recently promising results in LEEC devices [42]. As both emitters are ionic, in principle there is no need to incorporate additional mobile ions. A host–guest approach, using 1 wt % of **DiKTa-DPA-OBuIm** in **DiKTa-OBuIm** was also used, the latter acting as a host matrix for the former. The electroluminescence (EL) of the three device stacks is shown in Figure 5a. Similar to the PL, the EL spectra are broad and unstructured. The EL of **DiKTa-OBuIm** and **DiKTa-DPA-OBuIm** occurs at λ_{EL} of 534 and 656 nm, respectively. Both neat-film EL spectra are red-shifted from the solution state and the 1 wt % in mCP film PL spectra. The origin of this red shift could be ascribed to the presence of emissive aggregates in the emissive layer [19]. Interestingly, in the host–guest system the energy transfer is not complete and both molecules are responsible for the electroluminescence, with a λ_{EL} at 586 nm, between the emission of the neat films. *JVL* characterization (from −2 to 8 V) was carried out on the three stacks (Figure 5b–d). As it can be seen, the current density reaches high values, and the injection is primarily dominated by ohmic behavior. The device with **DiKTa-DPA-OBuIm** shows a steeper injection reaching values of

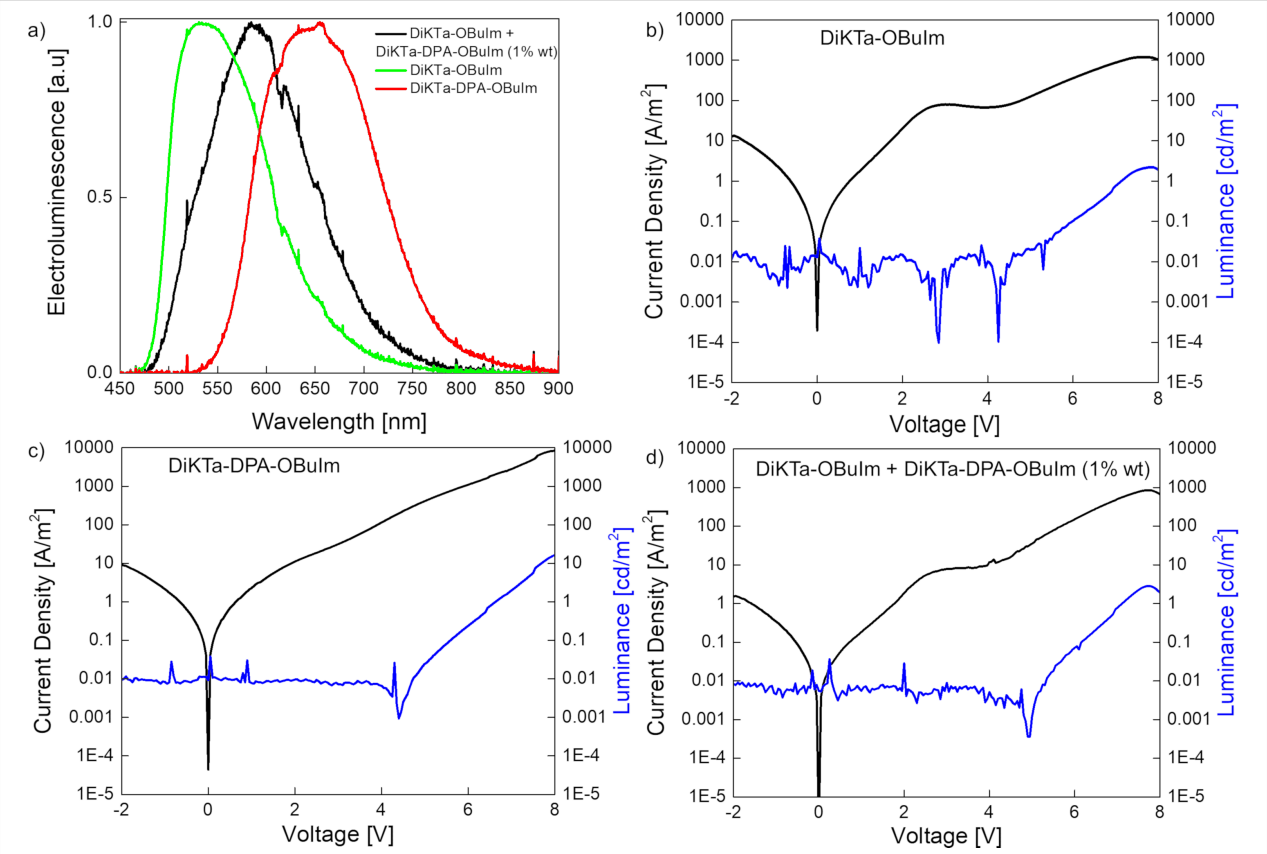

Figure 5: (a) Electroluminescence spectra of **DiKTa-OBuIm** (green curve), **DiKTa-DPA-OBuIm** (red curve) and 1% of **DiKTa-DPA-OBuIm** in **DiKTa-OBuIm** (black curve). Current (black) and luminance (blue) versus voltage (*JVL*) sweep (from −2 to 8 V) of (b) **DiKTa-OBuIm**, (c) **DiKTa-DPA-OBuIm**, and (d) 1% of **DiKTa-DPA-OBuIm** in **DiKTa-OBuIm**.

10,000 A m^{-2} at 8 V when compared with the device with **DiKTa-OBuIm**, which shows a current density of 1000 A m^{-2} at the same voltage value. The current density in the device with the host–guest system is dominated by the presence of **DiKTa-OBuIm**. Light emission is detected at around ≈5 V, with values of 15 cd m^{-2} for the device with **DiKTa-DPA-OBuIm** and around 2 cd m^{-2} for the devices with **DiKTa-OBuIm** and the host–guest system, each at 8 V. From the EL spectra it is possible to estimate the external quantum efficiency (EQE) values; however, they are also highly affected by the luminance levels, giving as a result very low efficiencies (<0.01%).

Conclusions

Two new ionic TADF emitters were designed and synthesized for LEECs application using a known MR-TADF emitter **DiKTa**. Our MR-TADF green emitter, **DiKTa-OBuIm** exhibited efficient green luminescence and TADF in 1 wt % mCP film (λ_{PL} = 499 nm, FWHM = 66 nm, Φ_{PL} = 71%, τ_d = 317 µs, k_{RISC} = 2.85 × 10^3 s^{-1}). This emitter represents a rare example of an ionic MR-TADF emitter for LEEC applications. The red emitter, **DiKTa-DPA-OBuIm**, was obtained by coupling a methoxy-modified diphenylamine unit onto the **DiKTa** fragment. Addition of a donor unit red-shifted the emission to red region with TADF (λ_{PL} = 577 nm, FWHM = 95 nm, Φ_{PL} = 61%, τ_d = 242 µs, k_{RISC} = 3.04 × 10^3 s^{-1}, 1 wt % in mCP). Different strategies were explored to prepare LEECs based on **DiKTa-OBuIm** and **DiKTa-DPA-OBuIm** as emitters. The devices showed green and red emission, respectively.

Supporting Information

The research data supporting this publication can be accessed at https://doi.org/10.17630/6ef45b8f-579d-4075-891e-595516c56e47.

Supporting Information File 1

^{1}H NMR and ^{13}C NMR spectra, GC–MS, and HRMS; supplementary computational data and coordinates; additional photophysical.
[https://www.beilstein-journals.org/bjoc/content/supplementary/1860-5397-18-136-S1.pdf]

Acknowledgements

We thank Dr. David Hall for providing help with the calculations and initial samples of some of the intermediates.

Funding

M. K. would like to thank 2214-A International Research Fellowship Programme for Ph.D. students (1059B141900585). This project has received funding from the European Union's Horizon 2020 research and innovation programme under the Marie Skłodowska Curie grant agreement No 838885 (NarrowbandSSL). S.M.S. acknowledges support from the Marie Skłodowska-Curie Individual Fellowship (grant agreement No 838885 NarrowbandSSL). A. K. G. is grateful to the Royal Society for Newton International Fellowship NF171163. L.M acknowledges that the project who gave rise to these results received support from the European Research Council (ERC) under the European Union's Horizon 2020 research and innovation programme Grant agreement No. 834431, the Spanish Ministry of Science, Innovation and Universities (MICIU, RTI2018-095362-A-I00, and EQC2018-004888-P) and the Comunitat Valenciana (IDIFEDER/2020/063 and PROMETEU/2020/077). D.T. acknowledges support from the Comunitat Valenciana (CIGE/2021/0).

ORCID® iDs

Merve Karaman - https://orcid.org/0000-0003-2803-7414
Abhishek Kumar Gupta - https://orcid.org/0000-0002-0203-6256
Tomas Matulaitis - https://orcid.org/0000-0003-0470-7356
Lorenzo Mardegan - https://orcid.org/0000-0002-9262-8094
Daniel Tordera - https://orcid.org/0000-0001-9283-8801
Henk J. Bolink - https://orcid.org/0000-0001-9784-6253
Ifor D. Samuel - https://orcid.org/0000-0001-7821-7208
Eli Zysman-Colman - https://orcid.org/0000-0001-7183-6022

Preprint

A non-peer-reviewed version of this article has been previously published as a preprint: doi:10.26434/chemrxiv-2022-n35w9-v3

References

1. Pei, Q.; Costa, R. D. *Adv. Funct. Mater.* **2020,** *30,* 2002879. doi:10.1002/adfm.202002879
2. van Reenen, S.; Matyba, P.; Dzwilewski, A.; Janssen, R. A. J.; Edman, L.; Kemerink, M. *J. Am. Chem. Soc.* **2010,** *132,* 13776–13781. doi:10.1021/ja1045555
3. Lindh, E. M.; Lundberg, P.; Lanz, T.; Edman, L. *Sci. Rep.* **2019,** *9,* 10433. doi:10.1038/s41598-019-46860-y
4. Youssef, K.; Li, Y.; O'Keeffe, S.; Li, L.; Pei, Q. *Adv. Funct. Mater.* **2020,** *30,* 1909102. doi:10.1002/adfm.201909102
5. Mindemark, J.; Edman, L. *J. Mater. Chem. C* **2016,** *4,* 420–432. doi:10.1039/c5tc03429a
6. Ràfols-Ribé, J.; Zhang, X.; Larsen, C.; Lundberg, P.; Lindh, E. M.; Mai, C. T.; Mindemark, J.; Gracia-Espino, E.; Edman, L. *Adv. Mater. (Weinheim, Ger.)* **2022,** *34,* 2107849. doi:10.1002/adma.202107849
7. Bai, R.; Meng, X.; Wang, X.; He, L. *Adv. Funct. Mater.* **2020,** *30,* 1907169. doi:10.1002/adfm.201907169
8. Zhang, C.; Liu, R.; Zhang, D.; Duan, L. *Adv. Funct. Mater.* **2020,** *30,* 1907156. doi:10.1002/adfm.201907156
9. Hu, T.; He, L.; Duan, L.; Qiu, Y. *J. Mater. Chem.* **2012,** *22,* 4206–4215. doi:10.1039/c2jm16185k
10. Housecroft, C. E.; Constable, E. C. *J. Mater. Chem. C* **2022,** *10,* 4456–4482. doi:10.1039/d1tc04028f
11. Costa, R. D.; Ortí, E.; Bolink, H. J.; Monti, F.; Accorsi, G.; Armaroli, N. *Angew. Chem., Int. Ed.* **2012,** *51,* 8178–8211. doi:10.1002/anie.201201471
12. Henwood, A. F.; Zysman-Colman, E. *Top. Curr. Chem.* **2016,** *374,* 36. doi:10.1007/s41061-016-0036-0
13. Kanagaraj, S.; Puthanveedu, A.; Choe, Y. *Adv. Funct. Mater.* **2020,** *30,* 1907126. doi:10.1002/adfm.201907126
14. Wong, M. Y.; Zysman-Colman, E. *Adv. Mater. (Weinheim, Ger.)* **2017,** *29,* 1605444. doi:10.1002/adma.201605444
15. Nakanotani, H.; Tsuchiya, Y.; Adachi, C. *Chem. Lett.* **2021,** *50,* 938–948. doi:10.1246/cl.200915
16. Wong, M. Y.; Hedley, G. J.; Xie, G.; Kölln, L. S.; Samuel, I. D. W.; Pertegás, A.; Bolink, H. J.; Zysman-Colman, E. *Chem. Mater.* **2015,** *27,* 6535–6542. doi:10.1021/acs.chemmater.5b03245
17. Uoyama, H.; Goushi, K.; Shizu, K.; Nomura, H.; Adachi, C. *Nature* **2012,** *492,* 234–238. doi:10.1038/nature11687
18. Pertegás, A.; Wong, M. Y.; Sessolo, M.; Zysman-Colman, E.; Bolink, H. J. *ECS J. Solid State Sci. Technol.* **2016,** *5,* R3160–R3163. doi:10.1149/2.0201601jss
19. Wong, M. Y.; La-Placa, M.-G.; Pertegas, A.; Bolink, H. J.; Zysman-Colman, E. *J. Mater. Chem. C* **2017,** *5,* 1699–1705. doi:10.1039/c6tc04821h
20. Lundberg, P.; Tsuchiya, Y.; Lindh, E. M.; Tang, S.; Adachi, C.; Edman, L. *Nat. Commun.* **2019,** *10,* 5307. doi:10.1038/s41467-019-13289-w
21. Lundberg, P.; Wei, Q.; Ge, Z.; Voit, B.; Reineke, S.; Edman, L. *J. Phys. Chem. Lett.* **2020,** *11,* 6227–6234. doi:10.1021/acs.jpclett.0c01506
22. Matsuki, K.; Pu, J.; Takenobu, T. *Adv. Funct. Mater.* **2020,** *30,* 1908641. doi:10.1002/adfm.201908641
23. Yu, R.; Song, Y.; Zhang, K.; Pang, X.; Tian, M.; He, L. *Adv. Funct. Mater.* **2022,** *32,* 2110623. doi:10.1002/adfm.202110623
24. Shen, H.-L.; Hsiao, P.-W.; Yi, R.-H.; Su, Y.-H.; Chen, Y.; Lu, C.-W.; Su, H.-C. *Dyes Pigm.* **2022,** *203,* 110346. doi:10.1016/j.dyepig.2022.110346
25. Hirai, H.; Nakajima, K.; Nakatsuka, S.; Shiren, K.; Ni, J.; Nomura, S.; Ikuta, T.; Hatakeyama, T. *Angew. Chem., Int. Ed.* **2015,** *54,* 13581–13585. doi:10.1002/anie.201506335
26. Madayanad Suresh, S.; Hall, D.; Beljonne, D.; Olivier, Y.; Zysman-Colman, E. *Adv. Funct. Mater.* **2020,** *30,* 1908677. doi:10.1002/adfm.201908677
27. Hall, D.; Suresh, S. M.; dos Santos, P. L.; Duda, E.; Bagnich, S.; Pershin, A.; Rajamalli, P.; Cordes, D. B.; Slawin, A. M. Z.; Beljonne, D.; Köhler, A.; Samuel, I. D. W.; Olivier, Y.; Zysman-Colman, E. *Adv. Opt. Mater.* **2020,** *8,* 1901627. doi:10.1002/adom.201901627
28. Wu, S.; Li, W.; Yoshida, K.; Hall, D.; Madayanad Suresh, S.; Sayner, T.; Gong, J.; Beljonne, D.; Olivier, Y.; Samuel, I. D. W.; Zysman-Colman, E. *ACS Appl. Mater. Interfaces* **2022,** *14,* 22341–22352. doi:10.1021/acsami.2c02756
29. Yuan, Y.; Tang, X.; Du, X.-Y.; Hu, Y.; Yu, Y.-J.; Jiang, Z.-Q.; Liao, L.-S.; Lee, S.-T. *Adv. Opt. Mater.* **2019,** *7,* 1801536. doi:10.1002/adom.201801536

30. Subeesh, M. S.; Shanmugasundaram, K.; Sunesh, C. D.; Chitumalla, R. K.; Jang, J.; Choe, Y. *J. Phys. Chem. C* **2016,** *120,* 12207–12217. doi:10.1021/acs.jpcc.6b03710
31. Tang, S.; Sandström, A.; Lundberg, P.; Lanz, T.; Larsen, C.; van Reenen, S.; Kemerink, M.; Edman, L. *Nat. Commun.* **2017,** *8,* 1190. doi:10.1038/s41467-017-01339-0
32. Connelly, N. G.; Geiger, W. E. *Chem. Rev.* **1996,** *96,* 877–910. doi:10.1021/cr940053x
33. Yan, C.; Shang, R.; Nakamoto, M.; Yamamoto, Y.; Adachi, Y. *Chem. Lett.* **2020,** *49,* 457–460. doi:10.1246/cl.200089
34. Yang, M.; Park, I. S.; Yasuda, T. *J. Am. Chem. Soc.* **2020,** *142,* 19468–19472. doi:10.1021/jacs.0c10081
35. Qi, Y.; Ning, W.; Zou, Y.; Cao, X.; Gong, S.; Yang, C. *Adv. Funct. Mater.* **2021,** *31,* 2102017. doi:10.1002/adfm.202102017
36. Xu, Y.; Li, C.; Li, Z.; Wang, Q.; Cai, X.; Wei, J.; Wang, Y. *Angew. Chem., Int. Ed.* **2020,** *59,* 17442–17446. doi:10.1002/anie.202007210
37. Serevičius, T.; Skaisgiris, R.; Dodonova, J.; Fiodorova, I.; Genevičius, K.; Tumkevičius, S.; Kazlauskas, K.; Juršėnas, S. *J. Phys. Chem. Lett.* **2022,** *13,* 1839–1844. doi:10.1021/acs.jpclett.1c03810
38. Melhuish, W. H. *J. Phys. Chem.* **1961,** *65,* 229–235. doi:10.1021/j100820a009
39. Tsuchiya, Y.; Diesing, S.; Bencheikh, F.; Wada, Y.; dos Santos, P. L.; Kaji, H.; Zysman-Colman, E.; Samuel, I. D. W.; Adachi, C. *J. Phys. Chem. A* **2021,** *125,* 8074–8089. doi:10.1021/acs.jpca.1c04056
40. Huang, F.; Wang, K.; Shi, Y.-Z.; Fan, X.-C.; Zhang, X.; Yu, J.; Lee, C.-S.; Zhang, X.-H. *ACS Appl. Mater. Interfaces* **2021,** *13,* 36089–36097. doi:10.1021/acsami.1c09743
41. Alahbakhshi, M.; Mishra, A.; Haroldson, R.; Ishteev, A.; Moon, J.; Gu, Q.; Slinker, J. D.; Zakhidov, A. A. *ACS Energy Lett.* **2019,** *4,* 2922–2928. doi:10.1021/acsenergylett.9b01925
42. John, J. C.; Shanmugasundaram, K.; Gopakumar, G.; Choe, Y. *ACS Photonics* **2022,** *9,* 203–210. doi:10.1021/acsphotonics.1c01397

License and Terms